MODELING IMMISCIBLE FLUID DISPLACEMENT IN A POROUS MEDIUM USING LATTICE BOLTZMANN METHOD

Magzhan Atykhan, B.Eng.

Submitted in fulfillment of the requirements

for the degree of Master of Science

in Mechanical & Aerospace Engineering

NAZARBAYEV UNIVERSITY

School of Engineering and Digital Sciences Department of Mechanical & Aerospace Engineering Nazarbayev University

53 Kabanbay Batyr Avenue,

Nur-Sultan city, Kazakhstan, 010000

Supervisor: Prof. Luis Rojas-Solórzano

Co-Supervisor: Prof. Desmond Adair

11.04.2021

DECLARATION

I hereby declare that this manuscript, entitled Modeling Immiscible Fluid Displacement in a Porous Medium Using Lattice Boltzmann Method," results from my work except for quotations and citations, which have been duly acknowledged.

I also declare that, to the best of my knowledge and belief, it has not been previously or concurrently submitted, in whole or in part, for any other degree or diploma at Nazarbayev University or any other national or international institution.

Name: Magzhan Atykhan

Date:11.04.2021

Abstract

The numerical analysis of the gas displacing immiscible liquid in 2D homogenous porous media is demonstrated. The model is analyzed in terms of different flow and pore geometry specifications, namely capillary number (Ca), liquid – gas viscosity ratio (D), surface wettability, and the pore domain's geometrical properties. The research intends to extend the understanding of complex multiphase flow in a porous domain with various physical parameters. The analysis was conducted using a 2D homogenous porous medium with seven-column circular- or square-shaped obstacles, representing the pores' solid wall. The model is constructed using pseudopotential Lattice Boltzmann Method (LBM) in Peng-Robinson's (P-R) EOS framework. One pore from the first column is removed to simulate more realistic flow behavior.

Additionally, small perturbations between neighboring pores were added. This work demonstrates that the gaseous phase penetration into the pore domain certainly depends on the aforementioned physical parameters. It was found that higher Ca and the surface wettability increases the effective gaseous phase penetration while increasing liquid-gas viscosity ratio leads to the opposite effect.

Acknowledgments

Firstly, I would like to express my immense thanks to Professor Luis Rojas-Solórzano for his valuable support, advice, and encouragement. His continuous guidance was priceless during the whole Master's degree.

Secondly, I would like to express special thanks to Mrs. Bagdagul Kabdenova (Dauyeshova) and Dr. Ernesto Monaco, Engineering Software Steyr (ESS), Austria their endless support and guidance throughout the project.

Finally, I would like to express my gratitude to Dr. M. Seaton for providing the original version of the DL MESO LBM package code.

Magzhan Atykhan

Table of Contents

List of Tables

List of Figures

Chapter 1 - Introduction

The growth of greenhouse gases (GHG) concentration in the atmosphere over the past centuries caused strong interest in developing technologies to reduce or sequestrate especially CO2 emissions. CO2 is primarily produced by fuel-burning during power and energy generation [1-3]. CO2 sequestration technology, which is part of the Carbon Dioxide Capture and Storage (CCS) project, is developed as one of the leading solutions to decrease CO2 concentration [4]. The concept of the technology is based on two main phases. Firstly carbon dioxide is captured from industrial and energy sources, then transported for further storage in an underground aquifer, commonly porous media isolated from the atmosphere [5-6]. Then, CO2 can be sequestrated by shear-driven force into smaller portions [7]. The displacement by the non-wetting phase by wetting phase is one of the most critical processes affecting CO2 storage in underground aquifers in terms of storage capacity, efficiency, and security [8-9]. However, it is a complicated phenomenon to study only in the laboratory or by analytical analysis. Therefore, numerical modeling is a complementary and powerful approach that can significantly help understand this phenomenon, provided the discretized model is capable of capturing the rich physics involved in such a process.

Generally, modeling and solving the phenomenon based on the conventional Navier-Stokes computational fluid dynamics (CFD) approach is challenging due to complex geometries and two-phase two-component systems. Simulation of CO2- brine flow in a porous domain can be done using several techniques: pore-scale models, core scale models, pilot-scale models, and field-scale models [9-10]. All models apart from pore-scale models are classified as continuum-scale models, and they describe macroscopic fluid flow in porous space. Therefore, Lattice Boltzmann Model (LBM) is used as the primary approach due to the capability to work with macro-scales difficulties [10]. The LBM models macroscopic fluid parameters based on its microscopic characteristics but avoids tracking every single molecule. In comparison with other CFD approaches, such as the volume of fluid (VOF) [11], the level set (LS) [12], and the phase-field (PF) [13], LBM has been successfully implemented in the accurate simulation of multiphase flows in porous media. Additionally, according to Yang and Boek [14], these CFD techniques have numerical instabilities at small-scale interface regions.

Another advantage of using LBM as a numerical tool in this research is that despite its memory consumption, its simplicity (every grid node generally only needs information from its immediate neighbor) makes the method very easy to be parallelized so the computational time

can be dramatically reduced [15-16]. Since the development of the method, multiple models have been developed [17-18], specifically the pseudopotential model, the color-fluid model, the mean-field theory, and the free-energy model. However, according to [19-22], all these models have limitations at high density and viscosity ratios due to spurious currents at the interface, which causes numerical instabilities. Fakhari and Rahiman [23] state that LBM multicomponent multiphase models can be used effectively only in limited gas-liquid density ratios (up to 15) due to numerical instability. Additionally, the model produces undesirable results if spurious currents' magnitude satisfies the local flow velocity [15].

Therefore, numerous studies were conducted to increase multiphase flow efficiency at high-density ratios in a porous domain. For instance, Yuan and Schaefer [26] found that using different EOS improves stability. It was stated that using Peng-Robinson (P-R) [30] and Carnahan-Starling (C-S) EOS can significantly enhance the model's stability. It correctly models the multiphase fluid flow process with an additional thermodynamic parameter such as temperature compared to other EOS. Other methods are based on calibrating the sound speed [24] and the interface thickness [25]. Moreover, Fakhari et al. [27] propose to appropriately calibrate inlet boundary conditions due to the model's vulnerability at the entrance.

Most LBM multiphase multicomponent studies on porous media were conducted using color-fluid LBM with a density ratio of 1 [6, 18, 28, 29]. However, it has been determined that the pseudopotential model has excellent capability in dealing with higher density ratios [26, 30]. The efficiency of the model subjects to EOS and the forcing scheme is examined in multiple research types [31-33, 26]. Depending on the introduction of interaction force into LBM, the forcing schemes are divided into three primary schemes: velocity-shift, exact difference method (EDM), and Guo's forcing scheme. Several studies were done to identify the stability and accuracy of schemes [17, 31-33]. Li et al. [31] found that EDM forcing scheme is more stable at relaxation time (τ) less than 1, and the velocity-shift forcing scheme is preferred when relaxation time equals 1, i.e., $\tau \approx 1$. However, Kupershtokh et al. [32] determined that at $\tau \approx 1$, both forcing schemes demonstrate the same results. It can be said that some contradictions can be caused due to the novelty of LBM. Consequently, we analyzed different forcing schemes concerning numerical stability and accuracy in this work.

In this study, the displacement process is analyzed using pseudopotential LBM rather than the widely applied color-fluid model. Additionally, P-R EOS, which is described by an acentric factor, is used due to its accuracy. During the work, the gaseous phase is injected into

the porous domain at different capillary numbers (Ca), viscosity ratios (D), and pore geometry. The efficiency of displacement is analyzed by manipulating these parameters. The density ratio is set at 5 to eliminate spurious current at the interface.

The paper is arranged as follows: Chapter 2 is dedicated to the multiphase LBM and P-R EOS, validation of the model is discussed in Chapter 3, Chapter 4 describes the analysis of displacement efficiency under different parameters. The conclusion is presented in Chapter 5.

Chapter 2 - Methodology

For this study, we used a standard LBE two-dimensional nine-level (D2Q9) model with Bhatnagar-Gross-Krook (BGK) collision operator, which characterizes the particle distribution function (PDF) in terms of space **x** and time t.

$$f_i(\boldsymbol{x} + \boldsymbol{e_i}\Delta t, t + \Delta t) = f_i(\boldsymbol{x}, t) + \frac{1}{\tau}(f_i^{eq}(\boldsymbol{x}, t) - f_i(\boldsymbol{x}, t)), (i = 0, 1 \ldots, M) \quad (1)$$

The streaming step is described on the left side of Equation 1, while the collision operator is presented on the right side. f_i is the particle velocity distribution, $\boldsymbol{e_i}$ is the microscopic velocity, and Δt is the time increment. τ expresses the dimensionless relaxation time, which is used to describe the kinematic viscosity $v = c_s^2(\tau - 0.5)\Delta t$. M is the number of discrete velocities and c_s is the speed of sound. f_i^{eq} is the corresponding equilibrium distribution function given by the following formula:

$$f_i^{eq}(\boldsymbol{x}, t) = \omega_i \rho[1 + 3(\boldsymbol{e_i u}) + \frac{9}{2}(\boldsymbol{e_i u})^2 - \frac{3}{2}\boldsymbol{u^2}] \quad (2)$$

where **u** denotes the macroscopic velocity and ω_i is the weighting factor. The schematic illustration of D2Q9 is given in Figure 1.

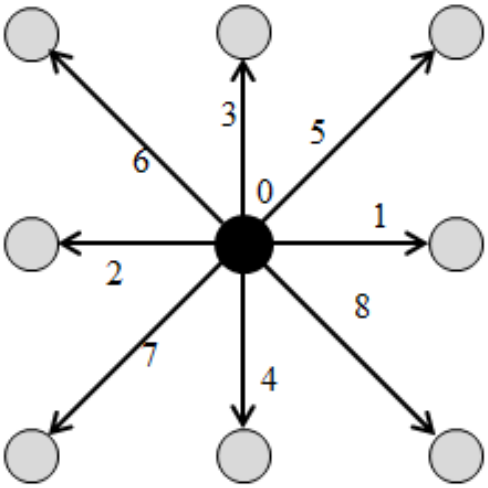

i	w*i*
0	4/9
2,4,6,8	1 /9
1,3,5,7	1/36

Figure 2.1. D2Q9 model and weighting factors

ρ describes the local mass density, and $\rho\boldsymbol{u}$ denotes local momentum density, Equations 3 and 4, respectively. The ideal EOS is defined in Equation 5.

$$\rho = \sum_i f_i \quad (3)$$

$$\rho\boldsymbol{u} = \sum_i f_i \boldsymbol{e_i} \quad (4)$$

$$p = c_s^2 \rho \quad (5)$$

In this project, the pseudopotential or Shan-Chen (S-C) model [34], which consists of body force depending on the discrete gradient of a density function, was used. The interaction force between neighboring nodes is described as follows:

$$\boldsymbol{F_{int}}(\boldsymbol{x}) = -\psi(\boldsymbol{x}) \sum_{\acute{x}} G(\boldsymbol{x}, \acute{\boldsymbol{x}}) \psi(\acute{\boldsymbol{x}})(\acute{\boldsymbol{x}} - \boldsymbol{x}) \quad (6)$$

where $G(\boldsymbol{x}, \acute{\boldsymbol{x}})$ is Green's function, which describes the interaction strength between neighbor nodes. The interaction force can be described as repulsive or attractive, depending on its magnitude. $\psi(\boldsymbol{x})$ is effective mass. The original SC model can be expressed by the general EOS:

$$p = c_s^2 \rho + \frac{c_s}{2} g[\psi(\rho)]^2 \quad (7)$$

The following equation expresses the adhesion force between two fluids.

$$F_{ads}(\boldsymbol{x}, t) = \text{-}G_{ads} \rho(\boldsymbol{x}, t) \sum_i \omega_i s\,(\boldsymbol{x} + \boldsymbol{e_i}\Delta t, t)\boldsymbol{e_i} \quad (8)$$

where, G_{ads} is adhesion parameter, which describes the interaction force between solid wall and fluid. The fluid can be considered non-wetting and wetting depending on its magnitude, specifically positive indicates non-wetting condition and negative expresses wetting condition [35]. The contact angle is calculated using the Young-Laplace equation [36]:

$$cos\theta = \frac{G_{ads,2} - G_{ads,1}}{G_c \frac{(\rho_1 - \rho_2)}{2}} \quad (9)$$

where, G_c is cohesion parameter, $\frac{(\rho_1 - \rho_2)}{2}$ is density factor.

The Shan-Chen EOS is used widely for LBM simulation due to its simplicity. However, in this study, for high-density ratios, Peng-Robinson EOS [37] is preferred (Equation 10 and 11). Additionally, P-R EOS reduces instability caused by spurious currents [26].

$$P = \frac{\rho RT}{1 - b\rho} - \frac{a\alpha(T)\rho^2}{1 + 2b\rho - b^2\rho^2} \quad (10)$$

$$\alpha(T) = [1 + (0.37464 + 1.54226\omega - 0.26992\omega^2) * \left(1 - \sqrt{\frac{T}{T_c}}\right)]^2 \quad (11)$$

where R is the universal gas constant, a ($a = 0.45724R^2T_c^2/p_c$) and b ($b = 0.0778RT_c/p_c$) are species-dependent coefficients, α denotes a function of reduced temperature ($T_r = \frac{T}{T_c}$, $T_c$is the critical temperature of species) and ω is an acentric factor. In this project, the values of a, b and R are 2/49, 2/21, and 1, respectively.

Chapter 3 - Validation of the model

Before starting the simulation, the model's validation has been performed using a capillary pressure test with expected analytical results. As shown in Figure 3.1, the gaseous phase penetrates two parallel passages with different widths. The top and bottom boundary conditions are on-grid bounce back, while inlet and outlet boundaries are defined as constant velocity and constant pressure correspondingly. Since the passages' width (r1 and r2) are not the same, the capillary pressure is different in passages (Pc1 and Pc2). The Young-Laplace equation is used to describe capillary pressure (Equation 12).

$$P_c = 2\sigma * \frac{\cos(\theta)}{r} \qquad (12)$$

where σ is the surface tension, and θ is the contact angle. Afterward, the results are analyzed with pressure difference (Δp) between the inlet (pin) and outlet (pout). According to conditions, the phase can penetrate or not into passages. When Δp is more significant than Pc1, the gaseous phase can flow through both passages, and the gas can only flow through Pc2 while Δp is in the range between Pc1 and Pc2. Lastly, the gas cannot penetrate both passages if Δp is less than Pc2.

For this study, contact angle equals θ=70o, viscosity ratio D = 1, and liquid-gas density ratio set to 5. The passages' widths (r1 and r2) are 15 and 30, respectively. Three different pressure differences are evaluated, specifically Δp1 = 1.04*10-3, Δp2 = 2.13*10-3, Δp3 = 4.3*10-3. Capillary pressures (Pc1 and Pc2) are calculated from Equation 12 and equals 2.51*10-3 and 1.25*10-3. Non-dimensional lattice units (lu) characterizes all these variables. The domain grid equals 280x140 $lu^{2,}$ and both passages have 100 lu in length. It can be seen from Figure 3.2. that the numerical solutions satisfy expected flow behavior.

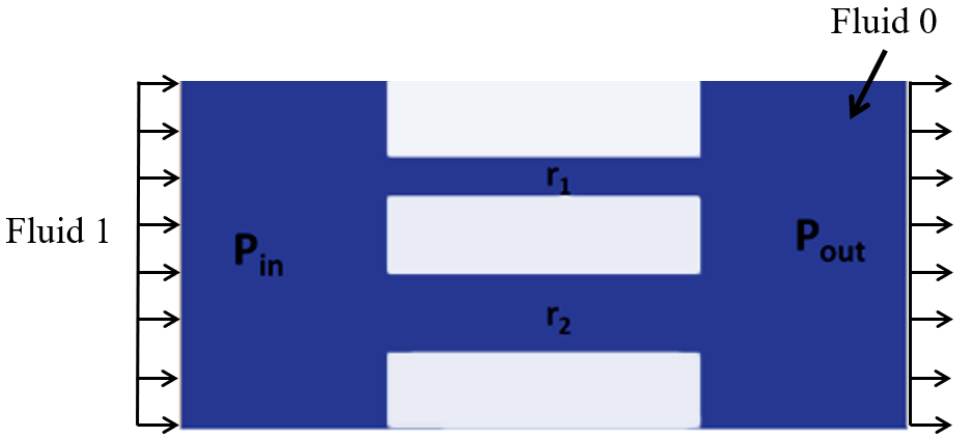

Figure 3.1. Initial domain grid for capillary pressure test.

Figure 3.2. Capillary pressure test results: a) $\Delta p1 = 1.04 * 10^{-3}$, b) $\Delta p2 = 2.13 * 10^{-3}$ and c) $\Delta p3 = 4.3 * 10^{-3}$.

Chapter 4 - Results and discussion

4.1. Model setup

The graphical illustration of the computational domain is presented in Figures 4.1 and 4.2. Top and bottom boundaries are periodic, while inlet and outlet are uniform velocity and constant pressure. The porous domain has 401 lu width and 401 lu length. The domain is occupied by circular pores with a radius of 10 lu (Figure 4.1) or 20x20 lu^2 square pores (Figure 4.2) separated with 10 lu passages. The pores are spatially located with small perturbation (±1 lu) to split flow uniformity throughout modeling and simulate more reasonable flow performance.

Moreover, in the 1st column, one pore is eliminated to analyze its impact on the fingering phenomenon. Initially, the pore domain is occupied by the liquid phase, and the gaseous phase is penetrated from left to right at a constant velocity. All cases are done at a constant liquid-gas density ratio of 5 and T_r of 0.95 (both parameters are related to a simulated fluid) to eliminate spurious currents [26].

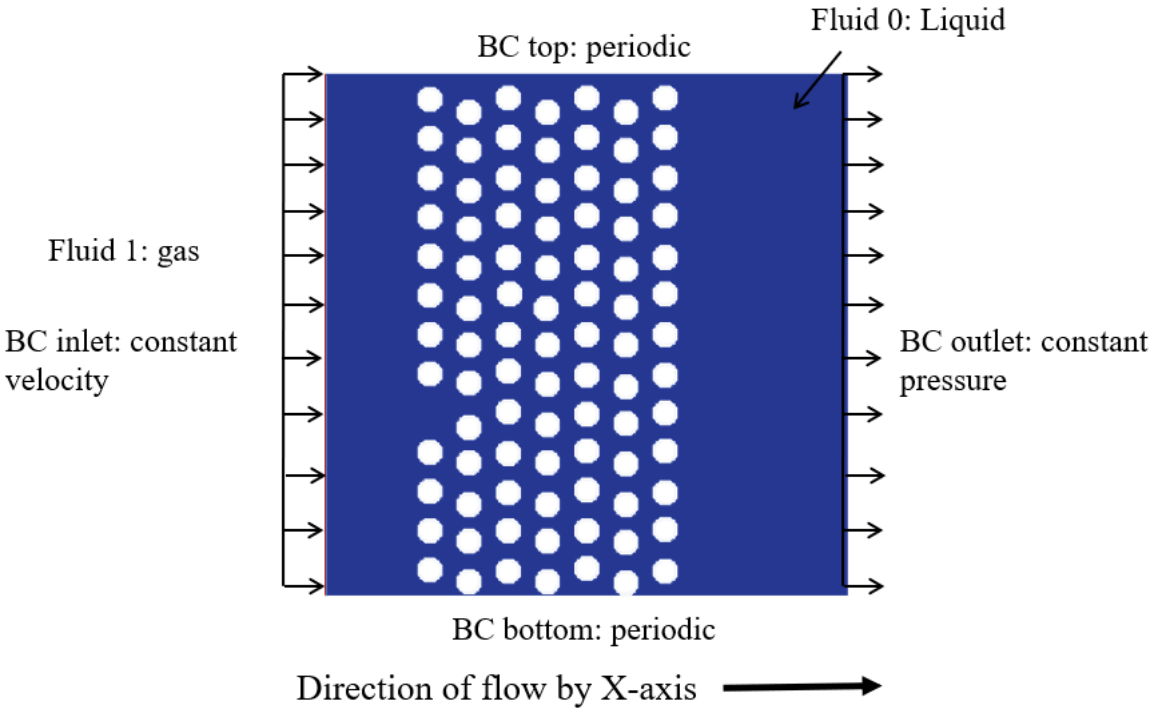

Figure 4.1. Illustration of 401x401 lu^2 domain filled with the circular pores (white circles are pores with radius = 10 lu)

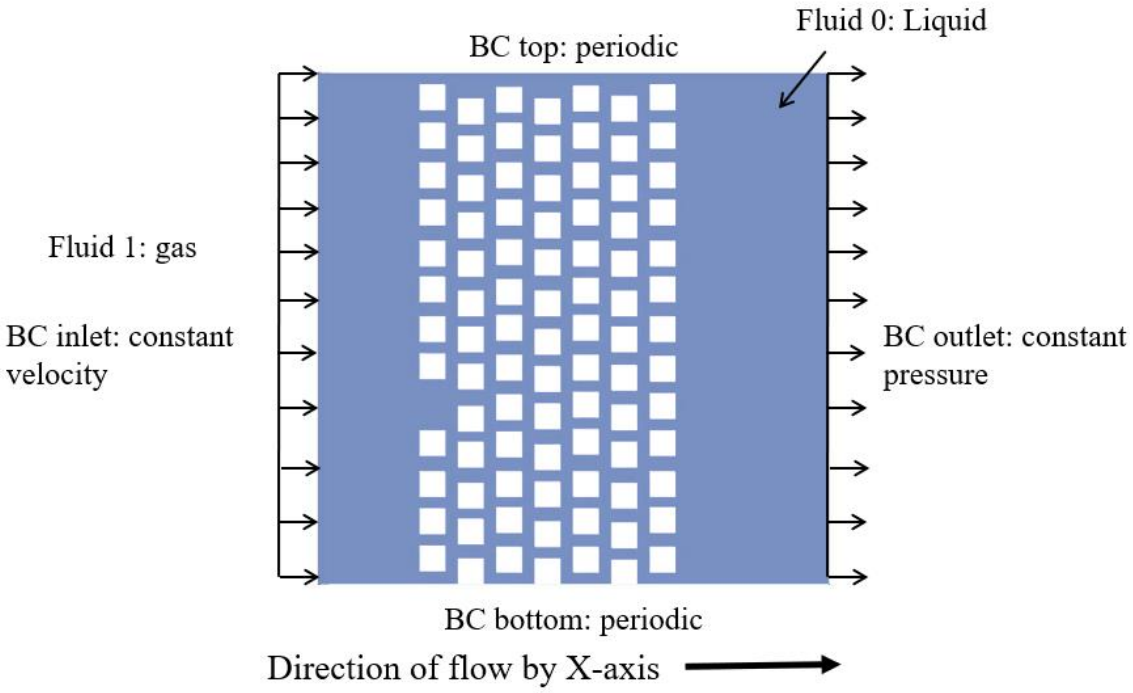

Figure 4.2. Illustration of 401x401 lu^2 domain filled with the square pores (white squares are pores with side = 20 lu).

As discussed before, the gaseous phase's penetration depends on multiple dimensionless parameters, precisely the Capillary number (Ca), the viscosity ratio (D), and surface wettability. The ratio of viscous and interfacial forces is presented by capillary number Ca:

$$C_a = \frac{u_G n_G}{\sigma} \qquad (13)$$

where u_G and n_G are the dynamic viscosity and the average velocity of Fluid 1 correspondingly. The viscosity ratio is described as the ratio of Fluid 0 and Fluid 1 viscosities:

$$D = \frac{n_L}{n_G} \qquad (14)$$

where n_L is the dynamic viscosity of the Fluid 0.

Moreover, a dimensionless time t* is introduced to avoid the effect of injected gaseous phase's velocity.

$$t^* = \frac{u_G * t}{H} \qquad (15)$$

where t defines the total time-steps and H is the domain's width.

4.2. Effect of forcing scheme

Firstly, before starting simulations, a forcing scheme analysis was done to guarantee its appropriate selection. For this reason, a circular-pore-based computational domain with $\theta = 70°$ and Ca = 0.038 was chosen. During this simulation, the velocity-shift and EDM forcing schemes were examined at $\tau = 1$. Figure 4.3 shows that both models have almost the same outcomes as was previously discussed. Therefore, the original velocity-shift forcing scheme at $\tau = 1$ was selected for the following simulations. However, it can be said that at low-temperature and low-viscosity ratio, which is not in the scope of this study, EDM forcing scheme is preferred due to improved numerical stability.

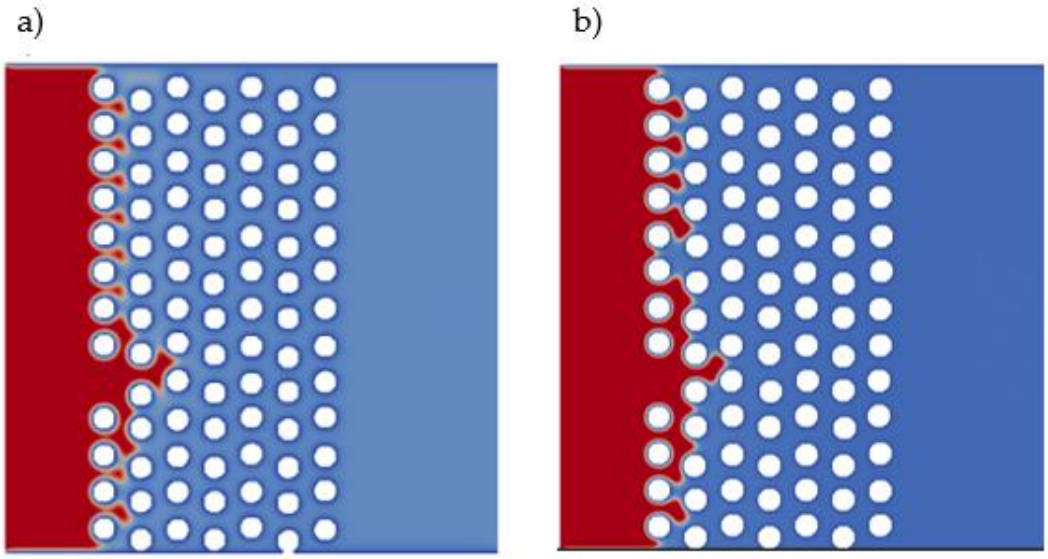

Figure 4.3. Illustration of Fluid 0 (red) evolution in circular pore domain at t* = 0.175, Ca = 0.038 and θ = 70° with: (a) velocity-shift forcing scheme and (b) EDM forcing scheme.

4.3. Effect of capillary number

Numerous simulations were conducted to analyze the influence of Ca on the gaseous phase penetration effectiveness. For this purpose, different Ca were selected, specifically Ca1 = 0.038, Ca2 = 0.076 and Ca3 = 0.115. The variation of Ca can be achieved by manipulating inlet velocity. Additionally, the D was selected as 1 and θ set to 70°, indicating wettable condition.

Figures 4.4 and 4.5 show that despite the same amount of fluid has been introduced at t* = 0.175 and different Ca, the penetration of the gaseous phase differs. Figures 4.4 and 4.5 show that higher Ca results in more effective penetration of the gaseous phase into the porous

domain, as was expected [30]. Furthermore, the fingering effect can be noticed for each selected pore geometry. Since lower entry pressure at a lower Ca (Figure 4.4a and Figure 4.5a), the fingering expands in the span-wise direction, while at higher Ca, the fingering favored the stream-wise direction. Lenormand et al. [38] found that low entry pressure can result in the backward evolution of capillary fingering. However, backward fingering is more common for a heterogeneous porous domain due to a higher difference in pore throat between neighboring pores [29].

Moreover, this study solves limitations denoted by Lenormand et al. [38]. They noticed that fluid occupies only a limited portion of the domain at higher Ca for a non-homogeneous porous media. Therefore, in this work, the model has periodic boundary conditions with uniform size and pores positioning, which neglects this drawback.

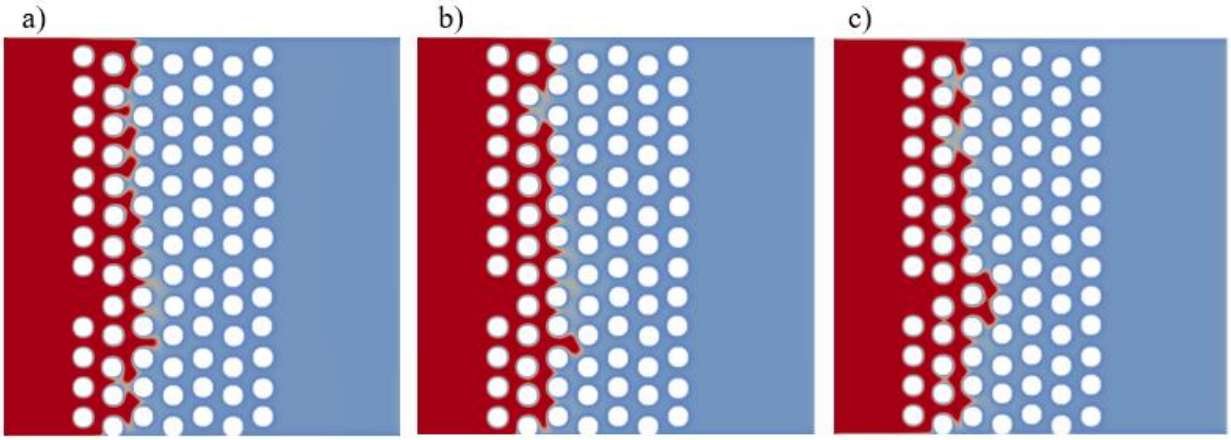

Figure 4.4. Illustration of Fluid 0 (red) evolution in circular pore domain at t* = 0.175 with different Ca: (a) Ca = 0.038; (b) Ca = 0.076 and (c) Ca = 0.115.

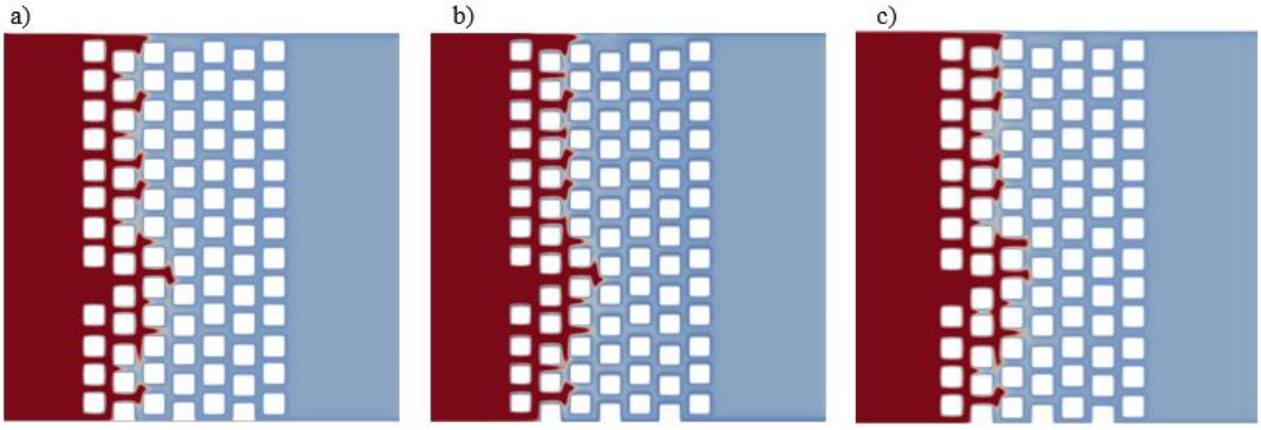

Figure 4.5. Illustration of Fluid 0 (red) evolution in square pore domain at t* = 0 .175 with different Ca: (a) Ca = 0.038; (b) Ca = 0.076 and (c) Ca = 0.115.

As shown in Table 4.1, the gaseous phase's penetration into the porous domain is affected by pore geometry. Figure 4.6 shows fluid evolution parameters: L denotes the domain length, the slip distance is S, and the effective penetration length is T. In this study, S is the constant for all cases.

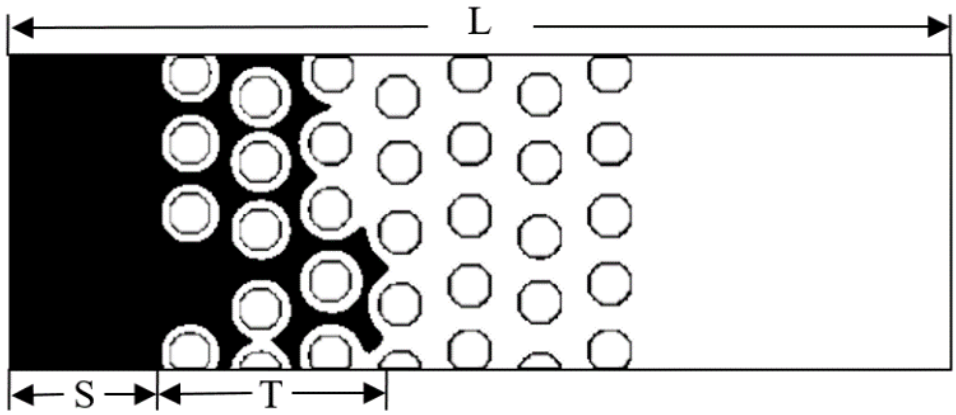

Figure 4.6. Graphical representation of gaseous phase penetration.

Table 4.1 illustrates that both pore geometries have approximately the same T at low Ca. However, the effective penetration length increases significantly in the square-shaped domain compared to circular-shaped. Additionally, it was found that excessively low Ca results on spurious currents related to numerical instabilities, as was noted by Raeini et al. [39]

Table 4.1. Results of penetration length T for different pore domains at various Ca and t* = 0.175.

Pore Geometry	**Ca**	**T (lu)**
Circular	0.038	84.322
Square	0.038	93.691
Circular	0.076	89.931
Square	0.076	97.447
Circular	0.115	92.812
Square	0.115	103.107

4.4. Effect of viscosity ratio

Moreover, viscosity ratio D is analyzed by manipulating Fluid 1 viscosity and keeping constant viscosity of Fluid 0. Furthermore, Ca is selected as 0.038, and θ is set as 70°. Figures 4.7 and 4.8 illustrate that a higher viscosity ratio makes the gas penetration more challenging. Additionally, it increases the time taken to displace the liquid phase from porous media. The results show that at low D, the fingering narrows, and as D increases, it thickens, as expected [18].

Additionally, our results show that the gas occupies only a fraction of the domain at low viscosity ratios, confirming previous results [30]. Also, increasing the viscosity ratio increases the displacement's stability (Figures 4.7c and 4.8c) [28]. It might be said that the pore geometry influences the gaseous phase penetration. In the square-shaped porous domain, T is longer than that in the circular-shaped domain, as shown in Table 4.2.

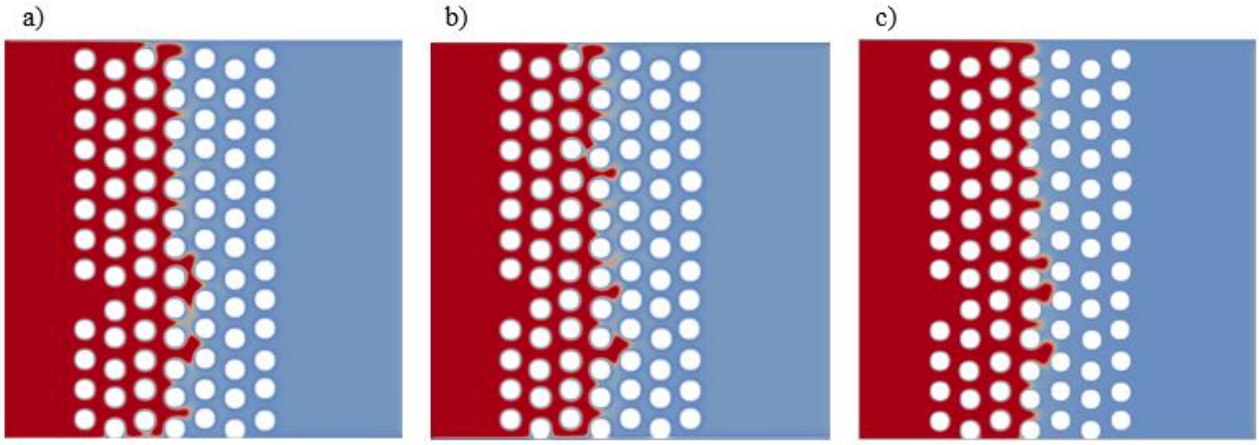

Figure 4.7. Illustration of Fluid 0 (red) evolution in circular pore domain at t* = 0.275, Ca = 0.038 and: (a) D = 1; (b) D = 2; (c) D = 3.

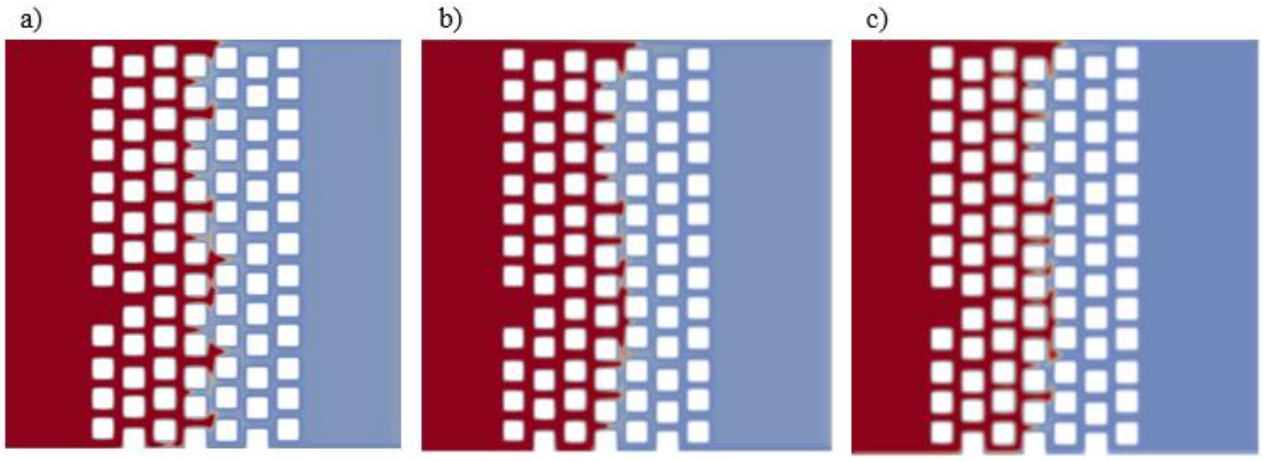

Figure 4.8. Illustration of Fluid 0 (red) evolution in square pore domain at t* = 0.275, Ca = 0.038 and: (a) D = 1; (b) D = 2; (c) D = 3.

Table 4.2. Results of penetration length T for different pore domains at various D and t* = 0.275.

Pore Geometry	**D**	**T (lu)**
Circular	1	119.937
Square	1	126.201
Circular	2	113.468
Square	2	118.933
Circular	3	106.619
Square	3	110.051

4.5. Effect of surface wettability

Lastly, the influence of surface wettability is examined by varying the contact angle between fluid and wall. As it was discussed before, according to capillary pressure (Equation 12), the penetration of the gaseous phase into the porous domain can be correctly determined. Therefore, the surface wettability, i.e., the surface contact angle, efficiently influences the gaseous phase's penetration into the porous media. A constant surface contact angle was used in previous studies on a porous domain [6, 18]. Consequently, in this work, numerous

simulations were conducted at varying surface contact angle, specifically θ = 83°, θ = 70°, θ = 50° and θ = 33° at constant Ca and D.

Figures 4.9 and 4.10 illustrate the gaseous phase's penetration into the liquid-filled domain at t* = 0.225. All models were carried out at wetting conditions, i.e., θ < 90°. Figures 4.9 and 4.10 demonstrate that the gaseous phase penetration length increases with decreasing surface contact angle, as was predicted [30]. Nevertheless, the effective gaseous phase evolution length is higher in circular-shaped (Figure 4.9) pore domain than in the square-shaped (Figure 4.10) pore domain because of the wider inter-pore passages (Figure 4.11).

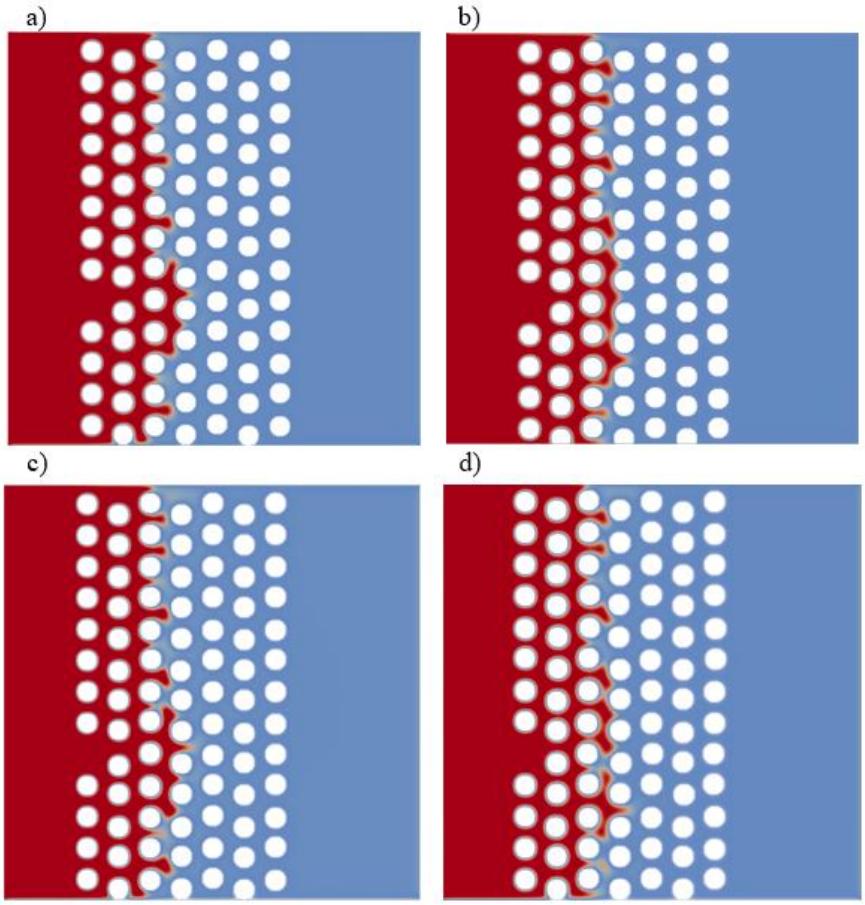

Figure 4.9. Illustration of Fluid 0 (red) evolution in circular pore domain at t* = 0.225 with fixed Ca = 0.038, D = 1 and: (a) θ = 83°; (b) θ = 70°; (c) θ = 50°; (d) θ = 33°.

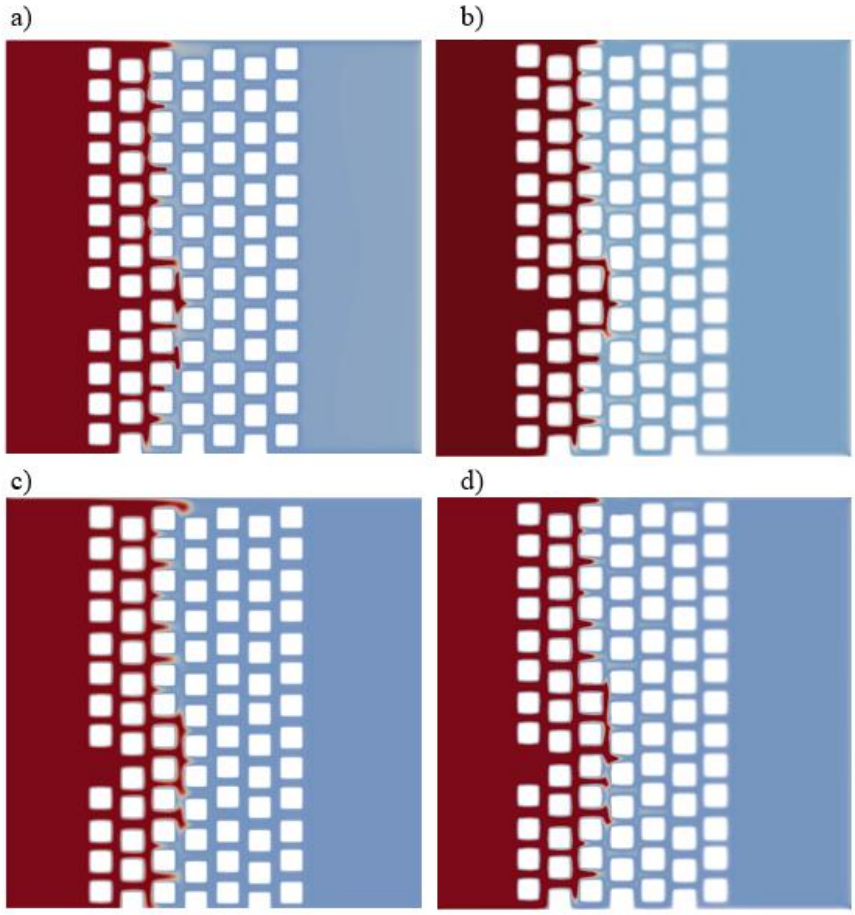

Figure 4.10. Illustration of Fluid 0 (red) evolution in square pore domain at t* = 0.225 time-step with fixed Ca = 0.038, D = 1 and: (a) θ = 83°; (b) θ = 70°; (c) θ = 50°; (d) θ = 33°.

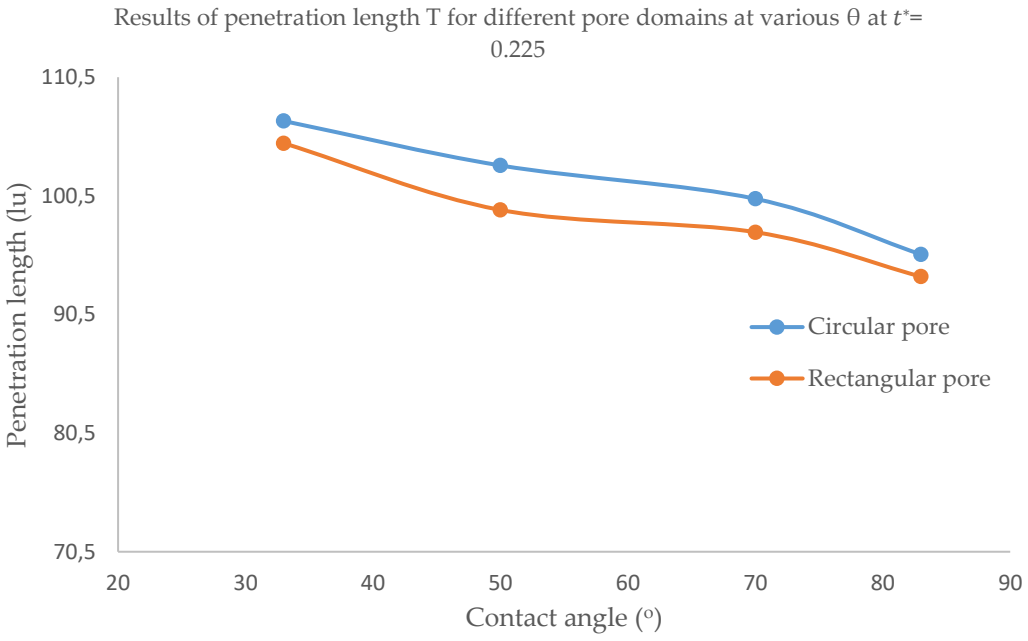

Figure 4.11. Results of penetration length T for different pore domains at various θ at t* = 0.225.

Chapter 5 – Conclusions

In conclusion, this work was done to identify the effect of Capillary number, viscosity ratio, and surface wettability on gaseous phase penetration into a 2D homogeneous liquid-filled porous domain. Previous works [6, 17, 27, 28] were conducted on the phase-field (PF) CFD method in collaboration with a color-fluid multiphase LBM model at a constant density ratio of 1. In this project, a pseudopotential LBM model with Peng-Robinson EOS was used to improve the model's numerical stability. Accordingly, P-R EOS makes it possible to model immiscible fluid displacement at a liquid-gas density ratio of 5 with insignificant numerical instabilities (i.e., spurious currents) at the interface. Moreover, the proper selection of forcing scheme increases the model's stability. It was determined that the velocity-shift and EDM forcing schemes have the same stability conditions at $\tau = 1$; hence, the velocity-shift forcing scheme was selected to simulate the models.

The numerical solutions indicated that the higher capillary number (Ca) and surface contact angle increase the gaseous phase penetration length for fixed viscosity ratio (D). The contrary effect can be noticed when D is increased with constant Ca and constant surface wettability. Moreover, the pore geometry affects the fingering length and effective gaseous phase penetration. In this work, the gaseous phase evolution length was lower in the circular-shaped pore domain than the square-shaped pore domain by about 10% and 4% with respect to Ca and D, respectively. However, at different surface contact angles, the square-pore domain's fingering length was less than 3% than that in the circular-shaped domain. Future research aims to examine gas-liquid displacement performance in a non-homogeneous porous medium with increasing the viscosity ratio. Additionally, in a future project, the EDM forcing scheme is planned to increase the model's stability at low relaxation times.

References

[1]. Otomo, H.; Fan, H.; Li, Y.; Dressler, M.; Staroselsky, I.; Zhang, R.; Chen, H. Studies of accurate multicomponent lattice Boltzmann models on benchmark cases required for engineering applications. J. Comput. Sci. 2016, 17, 334–339, doi:10.1016/j.jocs.2016.05.001.

[2]. Lal, R. Carbon sequestration. Philos. Trans. R. Soc. B Biol. Sci. 2007, 363, 815–830, doi:10.1098/rstb.2007.2185.

[3]. Tsang, C.; Benson, S.M.; Kobelski, B.; Smith, R.E. Scientific considerations related to regulation development for CO2 sequestration in brine formations. Environ. Earth Sci. 2002, 42, 275–281, doi:10.1007/s00254-001-0497-4.

[4]. Saxena, R.; Singh, V.K.; Kumar, E.A.; Kumar, E.A. Carbon Dioxide Capture and Sequestration by Adsorption on Activated Carbon. Energy Procedia 2014, 54, 320–329, doi:10.1016/j.egypro.2014.07.275.

[5]. Taghilou, M.; Rahimian, M.H. Investigation of two-phase flow in porous media using lattice Boltzmann method. Comput. Math. Appl. 2014, 67, 424–436, doi:10.1016/j.camwa.2013.08.005.

[6]. Liu, H.; Zhang, Y.; Valocchi, A.J. Lattice Boltzmann simulation of immiscible fluid displacement in porous media: Homogeneous versus heterogeneous pore network. Phys. Fluids 2015, 27, 052103, doi:10.1063/1.4921611.

[7]. Atykhan, M.; Kabdenova, B.; Rojas-Solórzano, L. ; and Monaco, E. "Lattice Boltzmann Model Simulation of Bubble Deformation and Breakup Induced by Micro-Scale Couette Flow", International Mechanical Engineering Congress and Exposition IMECE2020At: Virtual, Online, in Proceedings of the ASME 2020, 2020.

[8]. Yang, J.; Boek, E.S. A comparison study of multicomponent Lattice Boltzmann models for flow in porous media applications. Comput. Math. Appl. 2013, 65, 882–890, doi:10.1016/j.camwa.2012.11.022.

[9]. Begum, R.; Basit, MA Lattice Boltzmann Method and its Applications to Fluid Flow Problems. Eur. J. Sci. Res. 2008, 22, 216–231.

[10]. Gu, Q.; Liu, H.; Zhang, Y. Lattice Boltzmann Simulation of Immiscible Two-Phase Displacement in Two-Dimensional Berea Sandstone. Appl. Sci. 2018, 8, 1497, doi:10.3390/app8091497.

[11]. Hirt, C.; Nichols, B. Volume of fluid (VOF) method for the dynamics of free boundaries. J. Comput. Phys. 1981, 39, 201–225, doi:10.1016/0021-9991(81)90145-5.

[12]. Sussman, M.; Smereka, P.; Osher, S. A Level Set Approach for Computing Solutions to Incompressible Two-Phase Flow. J. Comput. Phys. 1994, 114, 146–159, doi:10.1006/jcph.1994.1155.

[13]. Jacqmin, D. Calculation of Two-Phase Navier–Stokes Flows Using Phase-Field Modeling. J. Comput. Phys. 1999, 155, 96–127, doi:10.1006/jcph.1999.6332.

[14]. Gunstensen, A.K.; Rothman, D.H.; Zaleski, S.; Zanetti, G. Lattice Boltzmann model of immiscible fluids. Phys. Rev. A 1991, 43, 4320–4327, doi:10.1103/physreva.43.4320.

[15]. Dauyeshova, B.K.; Rojas-Solórzano, L.R.; Monaco, E. Numerical simulation of diffusion process in T-shaped micromixer using Shan-Chen Lattice Boltzmann Method. Comput. Fluids 2018, 167, 229–240, doi:10.1016/j.compfluid.2018.03.029.

[16]. Meakin, P.; Tartakovsky, A.M. Modeling and simulation of pore-scale multiphase fluid flow and reactive transport in fractured and porous media. Rev. Geophys. 2009, 47, RG3002, doi:10.1029/2008rg000263.

[17]. Huang, H.; Krafczyk, M.; Lu, X. Forcing term in single-phase and Shan-Chen-type multiphase lattice Boltzmann models. Phys. Rev. E 2011, 84, 046710, doi:10.1103/physreve.84.046710.

[18]. Liu, H.; Valocchi, A.J.; Werth, C.J.; Kang, Q.; Oostrom, M. Pore-scale simulation of liquid CO2 displacement of water using a two-phase lattice Boltzmann model. Adv. Water Resour. 2014, 73, 144–158, doi:10.1016/j.advwatres.2014.07.010.

[19]. Holtzman, R. Effects of Pore-Scale Disorder on Fluid Displacement in Partially-Wettable Porous Media. Sci. Rep. 2016, 6, 36221, doi:10.1038/srep36221.

[20]. Hou, P.; Ju, Y.; Gao, F.; Wang, J.; He, J. Simulation and visualization of the displacement between CO2 and formation fluids at pore-scale levels and its application to the recovery of shale gas. Int. J. Coal Sci. Technol. 2016, 3, 351–369, doi:10.1007/s40789-016-0155-9.

[21]. Isfahani, A.M.; Afrand, M. Experiment and Lattice Boltzmann numerical study on nanofluids flow in a micromodel as porous medium. Phys. E Low-Dimens. Syst. Nanostructures 2017, 94, 15–21, doi:10.1016/j.physe.2017.07.008.

[22]. Tursynkhan, M.; Dauyeshova, B.; Adair, D.; Monaco, E.; Rojas-Solórzano, L. Simulation of Viscous Fingering in Microchannels With Hybrid-Patterned Surface Using Lattice Boltzmann Method. In Proceedings of the Volume 7: Fluids Engineering, ASME Meeting, Salt Lake City, UT, USA, 11–14 November 2019; doi:10.1115/IMECE2019-10876.

[23]. Fakhari, A.; Rahimian, M.H. Phase-field modeling by the method of lattice Boltzmann equations. Phys. Rev. E 2010, 81, 036707, doi:10.1103/physreve.81.036707.

[24]. Inamuro, T.; Yokoyama, T.; Tanaka, K.; Taniguchi, M. An improved lattice Boltzmann method for incompressible two-phase flows with large density differences. Comput. Fluids 2016, 137, 55–69, doi:10.1016/j.compfluid.2016.07.016.

[25]. Lee, T.; Liu, L. Lattice Boltzmann simulations of micron-scale drop impact on dry surfaces. J. Comput. Phys. 2010, 229, 8045–8063, doi:10.1016/j.jcp.2010.07.007.

[26]. Yuan, P.; Schaefer, L. Equations of state in a lattice Boltzmann model. Phys. Fluids 2006, 18, 042101, doi:10.1063/1.2187070.

[27]. Fakhari, A.; Li, Y.; Bolster, D.; Christensen, K.T. A phase-field lattice Boltzmann model for simulating multiphase flows in porous media: Application and comparison to experiments of CO2 sequestration at pore scale. Adv. Water Resour. 2018, 114, 119–134, doi:10.1016/j.advwatres.2018.02.005.

[28]. Liu, H.; Valocchi, A.; Kang, Q.; Werth, C.J. Pore-Scale Simulations of Gas Displacing Liquid in a Homogeneous Pore Network Using the Lattice Boltzmann Method. Transp. Porous Media 2013, 99, 555–580, doi:10.1007/s11242-013-0200-8.

[29]. Zhao, H.; Ning, Z.; Kang, Q.; Chen, L.; Zhao, T. Relative permeability of two immiscible fluids flowing through porous media determined by lattice Boltzmann method. Int. Commun. Heat Mass Transf. 2017, 85, 53–61, doi:10.1016/j.icheatmasstransfer.2017.04.020.

[30]. Atykhan, M.; Kabdenova (Dauyeshova), B.; Monaco, E.; and Rojas-Solórzano, L. R. "Modeling Immiscible Fluid Displacement in a Porous Medium Using Lattice Boltzmann Method," Fluids, 2021, 6 (2), 89-94. doi:10.3390/fluids6020089

[31]. Li, Q.; Luo, K.H.; Li, XJ Forcing scheme in pseudopotential lattice Boltzmann model for multiphase flows. Phys. Rev. E 2012, 86, 016709, doi:10.1103/physreve.86.016709.

[32]. Kupershtokh, A.; Medvedev, D.; I Karpov, D. On equations of state in a lattice Boltzmann method. Comput. Math. Appl. 2009, 58, 965–974, doi:10.1016/j.camwa.2009.02.024.

[33]. Chen, L.; Kang, Q.; Mu, Y.; Tong, Z.-X.; Tao, W.-Q. A critical review of the pseudopotential multiphase lattice Boltzmann model: Methods and applications. Int. J. Heat Mass Transf. 2014, 76, 210–236, doi:10.1016/j.ijheatmasstransfer.2014.04.032.

[34]. Shan, X.; Chen, H. Lattice Boltzmann model for simulating flows with multiple phases and components. Phys. Rev. E 1993, 47, 1815–1819, doi:10.1103/physreve.47.1815.

[35]. Martys, N.S.; Chen, H. Simulation of multicomponent fluids in complex three-dimensional geometries by the lattice Boltzmann method. Phys. Rev. E 1996, 53, 743–750, doi:10.1103/physreve.53.743.

[36]. Huang, H.; Thorne, D.T.; Schaap, M.G.; Sukop, M.C. Proposed approximation for contact angles in Shan-and-Chen-type multicomponent multiphase lattice Boltzmann models. Phys. Rev. E 2007, 76, 066701, doi:10.1103/physreve.76.066701.

[37]. Peng, D.-Y.; Robinson, D.B. A New Two-Constant Equation of State. Ind. Eng. Chem. Fundam. 1976, 15, 59–64, doi:10.1021/i160057a011.

[38]. Lenormand, R.; Touboul, E.; Zarcone, C. Numerical models and experiments on immiscible displacements in porous media. J. Fluid Mech. 1988, 189, 165–187, doi:10.1017/s0022112088000953.

[39]. Raeini, A.Q.; Bijeljic, B.; Blunt, M.J. Numerical Modelling of Sub-pore Scale Events in Two-Phase Flow Through Porous Media. Transp. Porous Media 2013, 101, 191–213, doi:10.1007/s11242-013-0239-6.